X- and *Q*-band ENDOR study of the Fe^+(II) center in chlorinated $SrCl_2$:Fe crystals

D. Ghica and S. V. Nistor
National Institute of Material Physics, POB MG-7 Magurele, 77125 Bucharest, Romania

H. Vrielinck and F. Callens
Department of Solid State Sciences, Ghent University, Krijgslaan 281, S1, B-9000 Gent, Belgium

D. Schoemaker
Physics Department, University of Antwerp, Universiteitsplein 1, B-2610 Antwerpen (Wilrijk), Belgium
(Received 3 March 2004; published 28 July 2004)

The ⟨001⟩ axially symmetric Fe^+(II) center observed in $SrCl_2$:Fe^{2+} crystals has been studied by the electron nuclear double resonance (ENDOR) technique in the microwave *X* and *Q* bands. This center is produced only in crystals grown in chlorine atmosphere and x-ray irradiated at low temperature (below 100 K). The analysis of the ENDOR spectra unambiguously confirms the structural model earlier suggested by the electron paramagnetic resonance (EPR) study, as a Fe^+ ion strongly displaced off center along an ⟨001⟩ axis, almost in the center of the square determined by the four nearest Cl^- ligands. The unpaired spin densities f_{3s} and f_{3p} in the 3*s* and 3*p* chlorine orbitals have been determined from the resulting ENDOR parameters.

DOI: 10.1103/PhysRevB.70.024105 PACS number(s): 76.30.Fc, 76.70.Dx, 61.72.Ji, 61.80.Cb

I. INTRODUCTION

Due to its cubic fluorite structure and unusually high ionic conductivity at high temperatures (around $T_C = 1000$ K), $SrCl_2$ is used as a simple model lattice to study the conduction mechanisms in the superionic state.[1,2] For such applications, it is very important to analyze the microstructure and dynamics of the point defects in the $SrCl_2$ lattice, the most appropriate technique being electron paramagnetic resonance (EPR).

An early EPR study on $SrCl_2$:Fe crystals grown in an inert atmosphere has shown[3] that x-ray irradiation at room temperature produces only cubic Fe^{3+} paramagnetic centers, which consist of a hole trapped at a substitutional Fe^{2+} impurity ion. An entirely different picture of the impurity type electron and hole trapping centers was found in chlorinated $SrCl_2$:Fe crystals, i.e., in crystals which were grown in a chlorine atmosphere. EPR studies on such crystals x-ray irradiated at low temperature (below 100 K) resulted in the identification of new iron based hole and electron trapping centers, namely, a trapped hole Fe^{3+} center with local trigonal symmetry[4] and the two trapped electron Fe^+(I) and Fe^+(II) centers, both with local tetragonal symmetry.[5] It was also found that the two tetragonal Fe^+ centers exhibit very different paramagnetic properties and thermal stability. Based on available EPR data, a substitutional eightfold coordination of the Fe^+ ion in the Fe^+(I) center and a strong ⟨001⟩ off-center displacement to a fourfold coordinated site in the Fe^+(II) center were proposed. Such structures would result in Γ_8 $\left(S=\frac{3}{2}\right)$ and Γ_5' $\left(S=\frac{1}{2}\right)$ ground states for the Fe^+(I) and Fe^+(II) centers, respectively, which could explain their different EPR properties.

The electron nuclear double resonance (ENDOR) study of the Fe^+(I) center, which was subsequently reported,[6] has confirmed the eightfold coordinated site of the interstitial Fe^+ ions. The tetragonal distortion has been attributed to the presence of monovalent impurity ions, very likely K^+, at the two opposite nearest-neighbor Sr^{2+} sites, along the tetragonal axis of the center.

As will be reported here, the *X*- and *Q*-band ENDOR study of the Fe^+(II) center in chlorinated $SrCl_2$:Fe crystals confirms the off-center position of the Fe^+ ion (d^7), very close to the center of the face formed by the four Cl^- ligands surrounding the cation lattice site and intersected by the tetragonal distortion axis, forming a kind of $(FeCl_4)^{3-}$ molecular ion. The charge transfer at the first shell of Cl^- ligands and the possible mechanism of this large ⟨001⟩ off-center displacement of the impurity ion are also discussed.

II. EXPERIMENTAL

$SrCl_2$ single crystals doped with Fe^{2+} were grown using the Bridgman technique in a chlorine atmosphere, as described in Ref. 4. For the magnetic resonance measurements, the crystals were cleaved with the long edge along a crystal ⟨110⟩ direction. In this way the angular dependence of the spectra could be recorded in a {110} plane. Typical sample sizes were $3\times3\times10$ mm^3 in the *X* band and $1\times1\times5$ mm^3 in the *Q* band.

The Fe^+(II) centers were produced by irradiation of the samples with x rays (Tungsten anticathode x-ray tube, operated at 60 kV and 40 mA) at $T=80$ K for typically half an hour. After x-ray irradiation the samples were transferred to the microwave cavity without raising their temperature above 100 K. The samples were oriented in the EPR cavity by inspection of the Fe^+(I) EPR spectrum, within a general accuracy of ±0.5°.

The *X*-band ENDOR measurements were performed on a BRUKER ESP300E spectrometer with a Bruker ESP353E ENDOR/TRIPLE extension [EN374 radio frequency (rf) amplifier and EN525 Schomandl synthesizer] equipped with

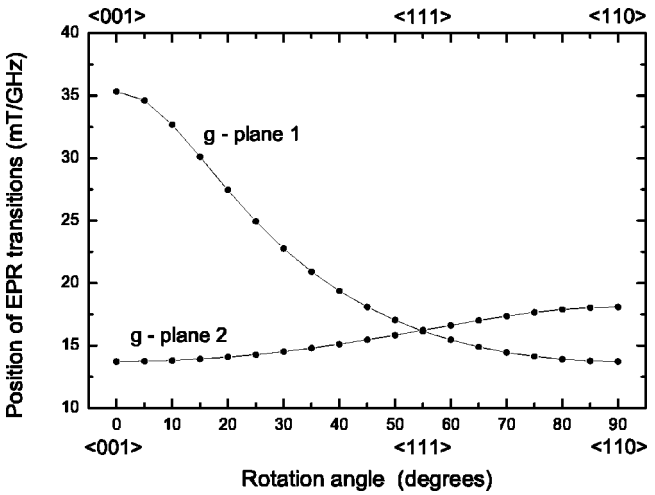

FIG. 1. EPR angular variation in a {110} plane of the Fe^+(II) center in $SrCl_2$:Fe. The positions of the EPR transitions are normalized to the microwave frequency as a result of our *X*-band (9.56 GHz) and *Q*-band (34.00 GHz) measurements.

an Oxford ESR10 flow cryostat. The *Q*-band ENDOR spectra were recorded using a BRUKER ELEXSYS E500 spectrometer, equipped with an Oxford CF935 cryostat. The best ENDOR spectra were recorded around 7 K in both the *X* and *Q* bands.

III. RESULTS

A. EPR results

The EPR study[5] on the Fe^+(II) center in $SrCl_2$:Fe crystals has shown that this center has tetragonal symmetry and can be described as a $S=\frac{1}{2}$ system with the following $\vec{\vec{g}}$ components: $g_{\parallel}=2.020$ and $g_{\perp}=5.211$. The corresponding EPR angular variation in a {110} plane is presented in Fig. 1. There are three magnetically inequivalent symmetry related orientations of the tetragonal Fe^+(II) centers in the cubic $SrCl_2$ lattice. The centers which have their tetragonal axis in the rotation plane {110} produce the angular dependence defined by us as *g*-plane 1. The other two orientations of the tetragonal axis are equivalent when the magnetic field is rotated in a {110} plane and they produce the angular dependence defined as *g*-plane 2. A similar notation of the angular variation of the EPR lines was used in the ENDOR study of the Fe^+(I) center (Ref. 6).

It is worthwhile mentioning at this point that after the low-temperature irradiation, on both sides of the most intense EPR lines attributed to the Fe^+(II) center one observes several less intense lines, very likely from other unstudied Fe^+-type centers. For one of these centers the angular dependence of the EPR transitions is very similar to that of the Fe^+(II), but it has a slightly different $\vec{\vec{g}}$ tensor. This new center, called here Fe^+(IIa), seems to be a Fe^+(II) center perturbed by some weakly interacting neighboring defect. As some of its EPR lines are overlapping on the low field side the EPR lines of the main Fe^+(II) center for orientations of the magnetic field close to the ⟨001⟩ direction, we took special precautions to avoid the presence of transitions originating from Fe^+(IIa), by recording the ENDOR spectra saturating at the high field side of the Fe^+(II) EPR line. The Fe^+(IIa) center will not be further analyzed here.

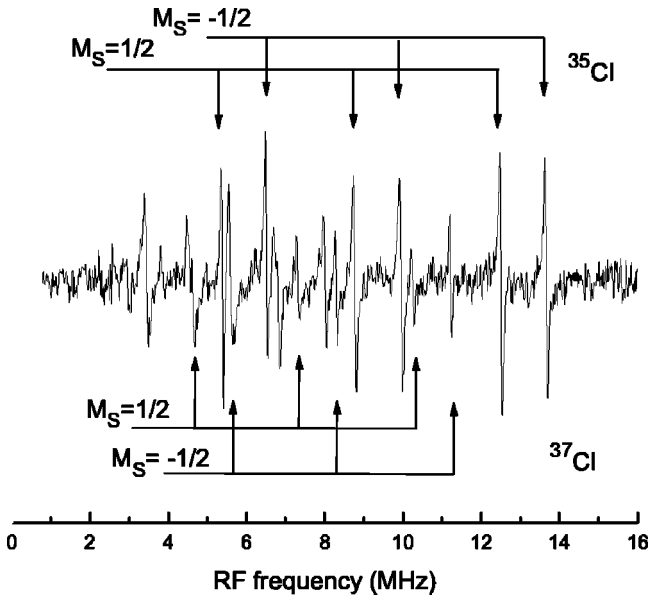

FIG. 2. *X*-band (9.56 GHz) ENDOR spectrum with $\mathbf{B}\|\langle 110\rangle$ in *g*-plane 1. All ENDOR transitions are attributed to the first $^{35}Cl/^{37}Cl$ shell interaction. The ^{35}Cl and ^{37}Cl ENDOR transitions corresponding to the *zz* components of the SHF interaction tensors are indicated with arrows.

B. First shell Cl interactions

The complete angular variation of the ENDOR spectra in the *X* and *Q* bands, in both *g*-plane 1 and *g*-plane 2 (shown in Fig. 1) has been recorded for this center, by rotating the crystal in a {110} plane. The most intense transitions have been assigned to the interaction with four equivalent ^{35}Cl (75.77%, $I=\frac{3}{2}$, $g_N=0.5479157$)/^{37}Cl (24.23%, $I=\frac{3}{2}$, $g_N=0.4560820$) nuclei, as shown in Fig. 2. The experimental *X*- and *Q*-band angular variations of the ENDOR spectrum for the ^{35}Cl isotope are presented in Figs. 3 and 4 along with their simulations.

As shown in Figs. 3(a) and 4(a), the angular variation of the *X*-band ENDOR transitions corresponding to the first ligands shell interaction has been very well fitted with the spin Hamiltonian[7]

$$\hat{H}_S = \mu_B \mathbf{B}\cdot\vec{\vec{g}}\cdot\hat{\mathbf{S}} + \hat{\mathbf{S}}\cdot\vec{\vec{A}}\cdot\hat{\mathbf{I}} - \mathbf{g}_N\mu_N\mathbf{B}\cdot\hat{\mathbf{I}} + \hat{\mathbf{I}}\cdot\vec{\vec{Q}}\cdot\hat{\mathbf{I}}, \quad (1)$$

where $S=\frac{1}{2}$, $I=\frac{3}{2}$ and the electronic $\vec{\vec{g}}$ components are known from the EPR measurements.

We obtained a high accuracy for the resulting superhyperfine (SHF) $\vec{\vec{A}}$ and $\vec{\vec{Q}}$ tensor components by including in the analysis the observed *X*-band ENDOR forbidden transitions ($\Delta M_S=0, \Delta M_I=2$), as well. The resulting ENDOR parameters (Table I) were further used to simulate the *Q*-band angular dependence in both *g* planes. The excellent fit with experimental data [Figs. 3(b) and 4(b)] confirms the correctness of the *X*-band ENDOR data analysis.

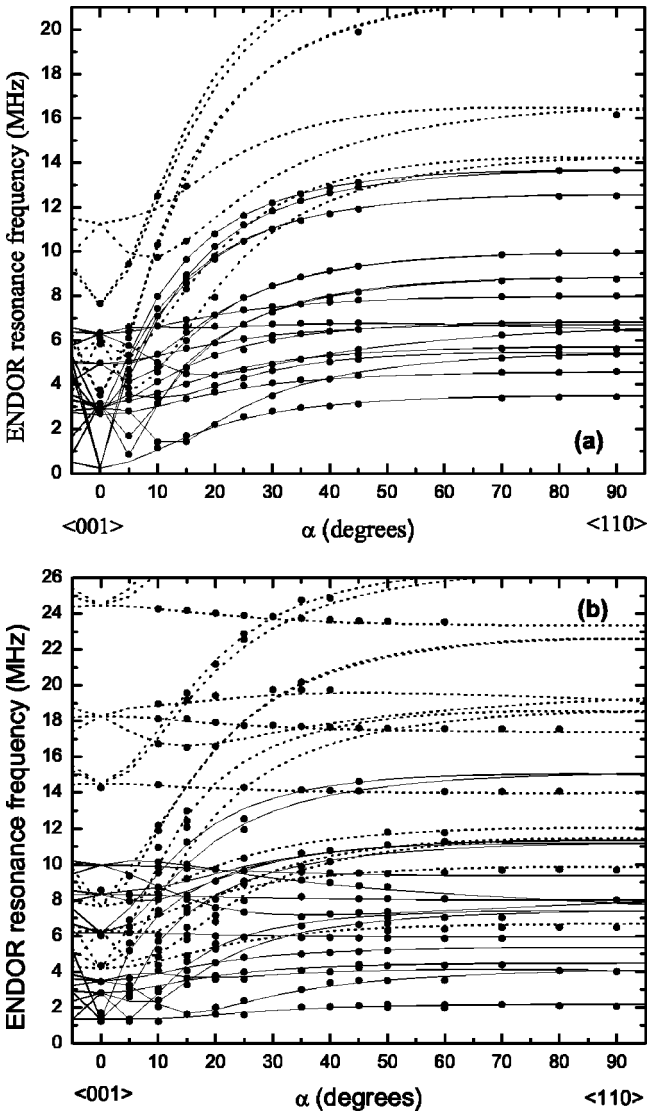

FIG. 3. ENDOR angular variation for the ^{35}Cl isotope in *g*-plane 1 in (a) *X* band (9.56 GHz) and (b) *Q* band (34.00 GHz). The experimental data are represented by filled circles. Simulated angular variations are represented by full lines for the allowed transitions ($\Delta M_I=1$) and dashed lines for the forbidden transitions [$\Delta M_I=2$ in (a) and $\Delta M_I=2,3$ in (b)].

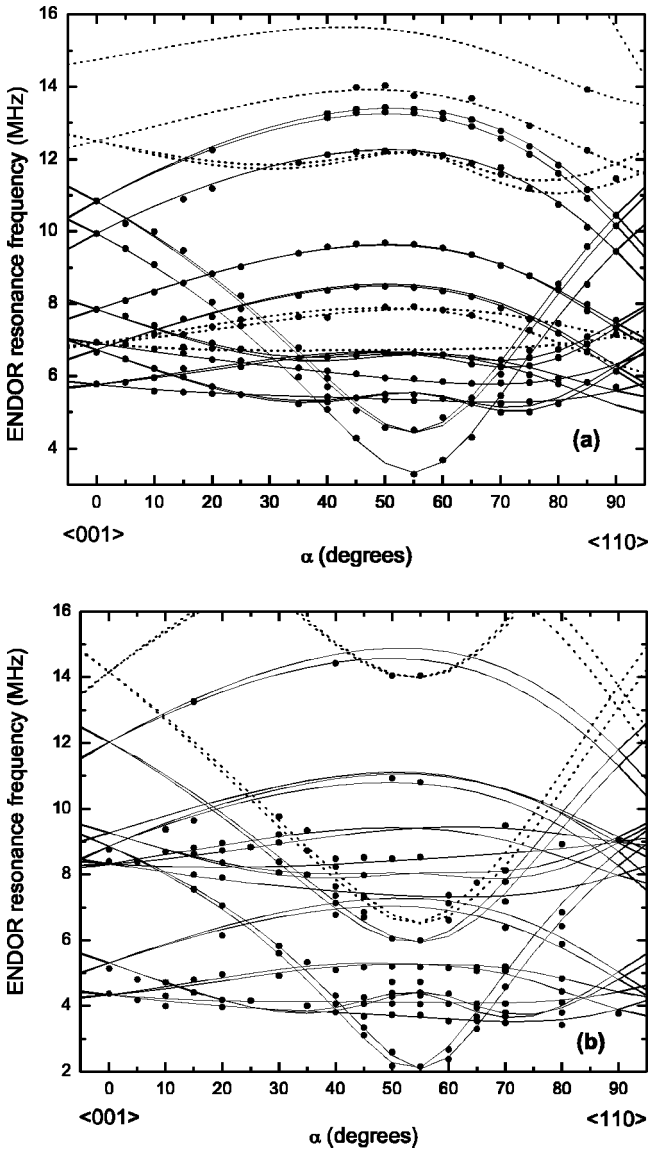

FIG. 4. ENDOR angular variation for the ^{35}Cl isotope in *g*-plane 2 in (a) *X* band (9.56 GHz) and (b) *Q* band (34.00 GHz). The experimental data are represented by filled circles. Simulated angular variations are represented by full lines for the allowed transitions ($\Delta M_I=1$) and dashed lines for the forbidden transitions [$\Delta M_I=2$ in (a) and $\Delta M_I=2,3$ in (b)].

The ENDOR angular dependence of the first Cl shell transition has been explained using the structural model which resulted from the EPR analysis and is presented in Fig. 5. According to this model, the Fe^{+} ion, resulting from electron trapping at a precursor Fe^{2+} ion, is strongly displaced from a normal Sr^{2+} cation site along the ⟨001⟩ axis, close to the center of four of the eight nearest Cl^{-} ligands. The tetragonal symmetry of the center imposes[8] that two principal axes of the SHF tensor $\overleftrightarrow{A}$, which we define as the *z* and *x* axes, lie in a {110} mirror plane, their orientations being defined by the angle θ_A. Usually, the SHF tensor *z* axis is oriented in the direction of the interconnection line between the center and the neighbor nucleus, i.e., along the Fe-Cl bond direction. In our case, the angle of the SHF tensor $\overleftrightarrow{A}$ is $\theta_A=2°$ (defined in Fig. 5), confirming that the Fe^{+} ion is indeed strongly displaced along the ⟨001⟩ axis, almost in the center of the square formed by the four nearest Cl^{-} ligands. The principal *z* and *x* axes of the quadrupole tensor $\overleftrightarrow{Q}$ are lying in the same {110} plane, but tilted at a different angle θ_Q (Table I). The combined effect of $\overleftrightarrow{A}$ and $\overleftrightarrow{Q}$ tensors axis tilting can be observed as a splitting of the corresponding ENDOR transitions when the magnetic filed is rotated away from the ⟨110⟩ direction.[9] The resulting orientation of the y_A and y_Q axes of the SHF tensor $\overleftrightarrow{A}$ and quadrupole tensor $\overleftrightarrow{Q}$, respectively, is normal to the {110} plane.

ENDOR gives no direct information concerning the total number of magnetically equivalent ligands, but the simulation of the SHF structure of an EPR line using the ENDOR

TABLE I. ENDOR parameters of the Fe^+(II) center in $SrCl_2$ for the first ^{35}Cl shell ligands. The SHF and quadrupole parameters of the corresponding ^{37}Cl nuclei are obtained by multiplying with the $g_N(^{37}Cl)/g_N(^{35}Cl)=0.8324$ and $Q(^{37}Cl)/Q(^{35}Cl)=0.7871$ ratios, respectively. The estimated errors are ±0.044 MHz for the principal values of the tensors and ±1° for the angles. The principal axes of the SHF tensors are defined in Fig. 5. The corresponding SHF interaction constants of both Fe^+(I) and Fe^+(II) centers in $SrCl_2$ are also included.

	Fe^+(II)		Fe^+(I)[a]
	$A_x=5.978$ MHz	$a=12.103$ MHz	$a=5.9$ MHz
SHF	$A_y=11.419$ MHz	$b=3.404$ MHz	$b=1.735$ MHz
interaction	$A_z=18.909$ MHz	$b'=-2.721$ MHz	$b'=-1.615$ MHz
	$\theta_A=2°$		
	$Q_x=0.670$ MHz	$q=-0.628$ MHz	$q=-0.92$ MHz
Quadrupole	$Q_y=0.586$ MHz	$q'=-0.042$ MHz	$q'=-0.06$ MHz
interaction	$Q_z=-1.256$ MHz		
	$\theta_Q=-8°$		

[a]Calculated from Ref. 6.

data allows us to determine unambiguously the number of equivalent nuclei interacting with the unpaired electron. With such a procedure, the 13 components structure observed in the EPR line of the Fe^+(II) center, at the $g_\perp$ position for the magnetic field parallel to the ⟨001⟩ direction, can be simulated with the SHF parameters given in Table I, by assuming a magnetic interaction with four equivalent $^{35}Cl/^{37}Cl$ nuclei (Fig. 6). By using a linewidth of 0.18 mT the resulting

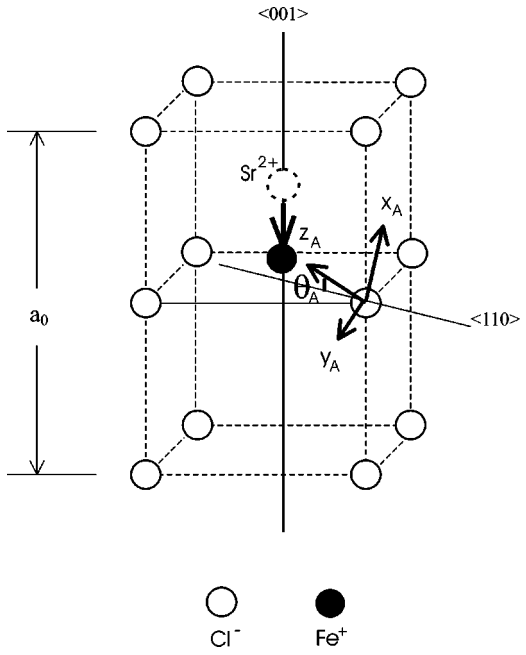

FIG. 5. Structural model of the Fe^+(II) center in chlorinated $SrCl_2$:Fe single crystals, based on a previous EPR study and the present ENDOR study of the SHF interaction with the first Cl shell. The orientation of the SHF tensor associated to one of the nearest four Cl nuclei is represented with x_A and z_A lying in the {110} plane and y_A normal to the {110} plane (details, see text).

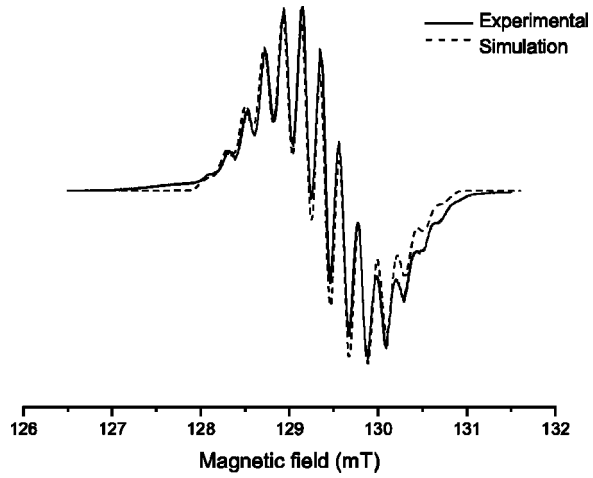

FIG. 6. Observed SHF structure of the EPR line at the $g_\perp$ position when $\mathbf{B}\|\langle 100\rangle$ (solid line) and the simulation of the SHF structure assuming an interaction with four equivalent $^{35}Cl/^{37}Cl$ nuclei (dashed line). The SHF splitting value was calculated from the $\vec{g}$ and $\vec{A}$ tensor data in the ⟨100⟩ direction.

superhyperfine splitting value of 0.214 mT, calculated from the $\vec{g}$ and $\vec{A}$ tensor data and used in the EPR spectrum simulation, agrees within the accuracy of the measurements with the observed splitting of 0.210 mT.

C. High-frequency ENDOR transitions

In addition to the transitions attributed to the interaction of the unpaired electrons with the nuclear moments of the first shell of Cl^- ligands, an additional group of two lines has been observed at higher rf frequencies in the *X*-band ENDOR spectrum in *g*-plane 1 when **B** is close to ⟨001⟩ (Fig. 7). The angular dependence of these lines (Fig. 7), which split when rotating the magnetic field away from the ⟨001⟩ direction, could only be followed in the {110} plane within an angular range of about 15° around the tetragonal axis. At larger angles they are overlapped by the more intense lines of the first Cl^- shell. All attempts to detect the corresponding lines in the *Q*-band ENDOR spectrum have been unsuccessful.

In order to identify the nature of the nucleus/nuclei responsible for these transitions we have applied the magnetic field shift method for two orientations in the magnetic field (⟨001⟩ and 12° away from ⟨001⟩ in *g*-plane 1). The resulting mean nuclear frequency f_N for both ENDOR lines at $B=350$ mT and for the two orientations is $f_N=13.79\pm0.95$ MHz, which is close to the nuclear frequency of the ^{19}F nucleus ($f_N=14.027$ MHz, $I=\frac{1}{2}$, 100%). These estimations were made by using the first order approximation in the case when the hyperfine interaction energy is much smaller than the nuclear Zeeman energy.[7] In agreement with this assumption the experimental high frequency ENDOR lines were found to be centered on the Larmor frequency of ^{19}F (Fig. 7).

As shown in Fig. 7, the angular dependence of these ENDOR lines is reasonably well reproduced considering the

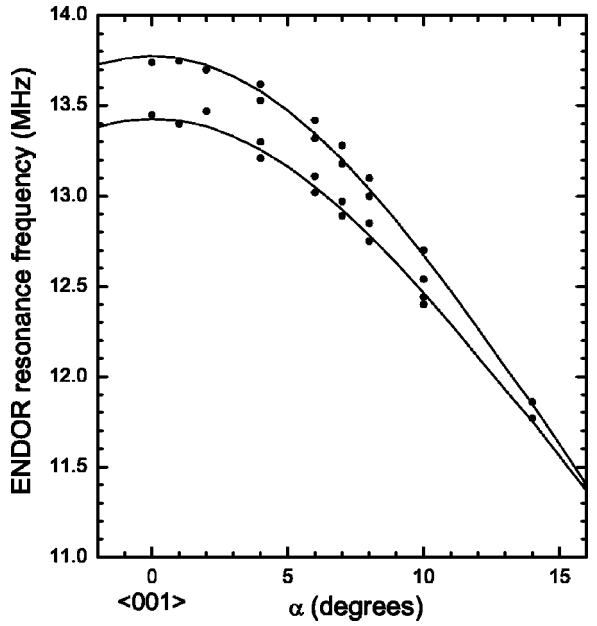

FIG. 7. *X*-band (9.56 GHz) experimental (full circles) and simulated (solid lines) ENDOR angular variation in *g*-plane 1 for one ^{19}F nucleus situated on the tetragonal axis.

interaction with one ^{19}F nucleus lying along the tetragonal axis, with the SHF components $A_z=0.35$ MHz and $A_x=A_y=-1.44$ MHz. Assuming that the anisotropic contribution to the SHF tensor is purely dipolar in nature, one obtains a Fe^+-axial defect separation of 0.625 nm, which is comparable to the lattice constant at room temperature $a_0=0.6978$ nm. The splitting of the two ENDOR lines, which is observed when rotating the magnetic field away from the $\langle 001\rangle$ direction, can be accounted for by considering that the interacting nucleus is not exactly located on the axis, but at a $(a,0,b)$ or (a,a,b) position in the lattice. The tetragonal symmetry of the center would than require that four such nuclei be present. However, in our opinion, the data are too limited to identify the interacting nucleus (nuclei) unambiguously.

IV. DISCUSSION

A. Covalency and bonding

The principal values of the SHF $\overleftrightarrow{A}$ tensor are related to the isotropic SHF constant a and the anisotropic SHF constants b and b' by[8]

$$A_x = a - b + b', \quad A_y = a - b - b', \quad A_z = a + 2b. \tag{2}$$

Similarly, the quadrupole interaction constants q and q' are related to the principal values of the quadrupole $\overleftrightarrow{Q}$ tensor by

$$Q_x = -q + q', \quad Q_y = -q - q', \quad Q_z = 2q. \tag{3}$$

The resulting SHF interaction constants corresponding to the first ^{35}Cl shell are presented in Table I, for both Fe^+-type centers.

In the case of the Fe^+(II) center, by considering the Fe^+ ion in the center of a square of four Cl^- ions, in the unrelaxed $SrCl_2$ lattice, the contribution of the magnetic point dipole-dipole interaction to the anisotropic SHF constant, for a Cl^--Fe^+ distance of $d=0.25a_0\sqrt{2}$, is $b_{dd}=1.344$ MHz. This means that the main contribution to the anisotropic SHF constant $b-b_{dd}=2.060$ MHz is due to covalency effects. In the previous EPR study of this center[5] a covalency factor $k=0.81$ was determined, which is typical for complexes with transition metal ions.[10] Here $k\sim 1-f$, where f is the fraction of unpaired electron spin transferred to the ligands. The experimental values of the isotropic and anisotropic SHF constants can be used to determine the unpaired spin densities f_{3s} and f_{3p} in the 3*s* and 3*p* chlorine orbitals, respectively,[8,11]

$$a = \frac{1}{2S} K f_{3s} |\psi_{3s}(0)|^2, \tag{4}$$

$$b - b_{dd} = \frac{1}{2S} K' f_{3p} \langle r^{-3}\rangle_{3p}, \tag{5}$$

where $K=\frac{2}{3}\mu_0 g_e \mu_B g_N \mu_N$ and $K'=(1/4\pi)\frac{2}{5}\mu_0 g_e \mu_B g_N \mu_N$. Using the values of $|\psi_{3s}(0)|^2$ and $\langle r^{-3}\rangle_{3p}$ for the Cl^- free ion,[12] one obtains $f_{3s}=0.27\%$ and $f_{3p}=1.95\%$. As shown in Table II, these values are in agreement with the general behavior of the covalency parameters given in literature for the d^7 ions $\left(S=\frac{1}{2}\right)$ with different neighboring ligands,[10,13,14] assuming[10,13] that $f_p \simeq f_\pi \simeq f_\sigma$.

TABLE II. Covalent bonding parameters for d^7 ions $\left(S=\frac{1}{2}\right)$ assuming that $f_p \simeq f_\pi \simeq f_\sigma$.

Ion	Lattice	d (nm)	f_s (%)	f_p (%)	Reference
Fe^+	NaF	0.231	0.29	1.45	11
	$SrCl_2$	0.247	0.27	1.95	present work
Co^{2+}	NaF	0.231	0.37	3.5	11
	$CdBr_2$	0.279[a]	0.57	5.3	12
	CdI_2	0.299[a]	0.54	7.5	12
Ni^{3+}	$KMgF_3$	0.199	0.60	9.25	11

[a]Calculated from the lattice constants and position of the atoms in the lattice.

Following Owen's calculations,[10] one can describe the orbital reduction factors in the case of a square-planar configuration with the formulas

$$k_{\pi\pi} \simeq 1 - 2f_\pi = 0.96,$$

$$k_{\sigma\pi} \simeq 1 - \frac{1}{2}[3f_\sigma + 4f_\pi + 3f_s + (12 f_\sigma f_\pi)^{1/2} - 6.47(f_\pi f_s)^{1/2}]$$

$$= 0.92.$$

Using the above formulas, again in the approximation of a perfect square configuration, one obtains a total covalency factor of $k=0.88$. Considering the various approximations employed in our calculations, this value is in good agreement with the $k=0.81$ value estimated from the EPR data, by using the simple theory of Tinkham.[15]

A similar analysis can be applied to the Fe^+(I) center as well. Assuming that the Fe^+ ion is situated in the center of a

cube of eight Cl^- ions, in the unrelaxed $SrCl_2$ lattice, one obtains a direct dipolar contribution $b_{dd}=0.506$ MHz. In this geometry, the Fe^+-Cl^- distance for the first shell of ligands is $d=0.25a_0\sqrt{3}$. It results in a charge transfer (covalency) contribution $b-b_{dd}=1.229$ MHz. In this case one would expect smaller SHF constants and contributions to covalence than in the case of the Fe^+(II) center. Indeed, the larger the Fe^+-Cl^- distance for the first shell of anions is, the smaller the SHF constants and covalency effects become. Taking into account that for this center the electronic spin is $S=\frac{3}{2}$, one obtains $f_{3s}=0.40\%$ and $f_{3p}=3.49\%$, indicating a stronger covalent character of the Fe^+-Cl^- bonding. In the case of the Fe^+(I) center, the higher electronic spin overcompensates the smaller SHF constants.

B. Structural model-formation mechanisms

The analysis of the ENDOR transitions from the first shell of Cl^- ligands, corroborated with the simulation of the SHF structure of the EPR spectrum, confirms the off-center structural model of the Fe^+(II) center. Moreover, the ENDOR results suggest that the the Fe^+ ion is only about 0.0082 nm (undistorted lattice) away from the center of one of the faces of the cube formed by the eight Cl^- ligands surrounding the cation site, which is intersected by the tetragonal axis of the paramagnetic center.

The mechanism behind this off-center displacement might either be extrinsic, involving the presence of a neighboring impurity along the tetragonal axis, or intrinsic, involving the minimization of the energy of the Fe^+ ion produced by electron trapping at the Fe^{2+} precursor. In the case of the extrinsic mechanism, the off-center displacement could be induced by a strong Coulombian interaction between a positively charged cation impurity lying along the tetragonal axis in the center of the next (lower in Fig. 5) normally empty cube of eight Cl^- ions, and the effectively negatively charged Fe^+ ion. Although such a cation impurity has not been detected by ENDOR, it does not mean that it could not exist. However, it is unlikely that it would allow the Fe^+ ion to move so close to it, at only 0.0082 nm from the center of the plane formed by the four nearest Cl^- ligands, as results from the analysis of the ENDOR data.

The observation of the high-frequency SHF interaction suggests the presence of a neighboring perturbing defect, containing most likely a ^{19}F nucleus, located further away, approximately along the tetragonal $\langle 100\rangle$ axis, or possibly of four such defects in either $(a,0,b)$ or (a,a,b) positions. Considering the large separating distance, as well as the screening effect of the intermediate Cl^- ligands, it is very unlikely that such a further lying defect could induce by its simple presence the observed strong off-center displacement of the Fe^+ ion. It is more likely that the defect(s) responsible for the high-frequency ENDOR lines play only a perturbing effect. In such a case, changes into the configuration/structure of these defect(s) would result in the presence of some extra EPR lines due to Fe^+(II)-like centers, with similar symmetry but slightly different $\vec{g}$ components. The presence of such lower intensity, satellite Fe^+(II)-like EPR lines, which are partly overlapping the spectrum of the main Fe^+(II) center for orientations close to $\mathbf{B}\|\langle 001\rangle$ in g-plane 1, has indeed been observed.

The existence of an intrinsic mechanism responsible for the observed strong off-center displacement of the Fe^+ ion (d^7) in the $SrCl_2$ lattice is supported by the observation of a similar effect in the case of the Ni^+ (d^9) ion in the CaF_2 crystals[16] with the same fluorite-type structure. From the analysis of the SHF interaction of the Ni^+ ion with the four nearest F^- ligands, it was found that the Ni^+ ion is also off-center displaced along the $\langle 001\rangle$ direction which intersects the plane containing the F^- ligands, at 0.037 nm from its center, corresponding to an angle of 79° between the tetragonal local axis and the Ni^+-F^- bond axis. The off-center displacement of the Ni^+ ion in the CaF_2 crystal lattice has been further confirmed by the analysis of the ENDOR spectra from the next two to seven shells of F^- ligands.[17] No additional ENDOR signals which could be attributed to the presence of some neighboring impurity responsible for the off-center displacement of the Ni^+ ion, have been reported.

The off-center displacement of the Ni^+ ion in CaF_2 has been explored through density functional theory calculations as well.[18] The analysis has shown that such large off-center displacement is possible, arising from the energy gain associated with the passing from eightfold to fourfold coordination.

In the case of an intrinsic mechanism, the off-center displacement of the extra negatively charged Fe^+ ion along a $\langle 001\rangle$ axis would result from a decrease in its energy by moving from the eightfold coordinated substitutional site, initially occupied by the Fe^{2+} precursor, into a fourfold coordinated site, at approximately the center of a face of the cube formed by the eight nearest Cl^- ligands. Such a displacement would be accompanied by a change in the structure of its lowest energy level, from a Γ_8 fourfold spin degenerate state in the eightfold coordinated site to a Γ_5' orbital triplet, which is further split into six Kramers doublets by the axial crystal field and the spin-orbit interactions. It is expected that such a site switching would be the result of a delicate balance between the electrostatic barrier, opposing the paramagnetic impurity displacement and the resulting energy gain by moving into the fourfold coordinated site. The same fine balance of forces may also explain why, contrary to the Fe^+(I) center, which is stabilized by the presence of nearest-neighbor K^+ cation impurities, being thus thermally stable up to 700 K, the Fe^+(II) center already decays at 150 K.

The available experimental data do not yield sufficient information to determine unambiguously which mechanism is responsible for the observed off-center displacement. It may be even possible that a combination of both is present, some perturbing neighboring defect favoring the off-center displacement. It is, however, worth mentioning that the intrinsic off-center displacement of the cation impurity ions along a $\langle 001\rangle$ axis seems to be a characteristic of the fluorite-type crystal lattice, as it has been also reported in the case of the Cu^{2+} and Ag^{2+} d^9 ions in $SrCl_2$ crystals.[19,20] Although both divalent cations are well known candidates for the Jahn-Teller (JT) effect, the observed intrinsic off-center stabilization has been attributed[21] to the energy lowering related with

the formation of a strongly covalent $(MeCl_4)^{2-}$ complex perturbed by the surrounding host matrix.

V. CONCLUSIONS

The present ENDOR study confirms the earlier proposed structural model of the Fe^+(II) center, based on EPR data, as a Fe^+ ion strongly displaced off-center along the ⟨001⟩ axis, very close to the center of its intersection point with the corresponding face of the cube formed by the eight nearest Cl^- ligands. The analysis of the ENDOR data also suggests that the off-center displacement of the Fe^+ ion is mainly due to an intrinsic mechanism, as previously observed in the case of some paramagnetic $3d^9$ transition ions in fluorite-type $SrCl_2$ and CaF_2 crystals.[16,19,20] In this respect, the defect which is responsible for the incomplete high frequency ENDOR spectrum seems to play only a perturbing effect in the formation/stabilisation of the Fe^+(II) center.

ACKNOWLEDGMENTS

This work was performed under the auspices of a Flemish-Romanian collaborative scientific research project (BIL96/57) and partially supported by the CNCSIS grant 613/2003. The Fund for Scientific Research - Flanders (Belgium) is acknowledged for financial support. One of us (H.V.) has been supported by the same institute with a grant.

[1] M. F. Butman, A. A. Smirnov, L. S. Kudin, and H. Dabringhaus, Surf. Sci. **511**, 331 (2002).
[2] J. Oberschmidt and D. Lazarus, Phys. Rev. B **21**, 2952 (1980).
[3] J. M. D. Siebenthal, D. Nicollin, and H. Bill, Chem. Phys. Lett. **58**, 317 (1978).
[4] S. V. Nistor, D. P. Lazar, H. Kaess, and D. Schoemaker, Solid State Commun. **104**, 521 (1997).
[5] S. V. Nistor, M. Stefan, and D. Schoemaker, Phys. Status Solidi B **214**, 229 (1999).
[6] H. Vrielinck, F. Callens, P. Matthys, S. V. Nistor, D. Ghica, and D. Schoemaker, Phys. Rev. B **64**, 024405 (2001).
[7] A. Abragam and B. Bleaney, *Electron Paramagnetic Resonance of Transition Ions* (Clarendon Press, Oxford, 1970).
[8] J. M. Spaeth, J. R. Niklas, and R. H. Bartram, *Structural Analysis of Point Defects in Solids. An Introduction to Multiple Magnetic Resonance Spectroscopy* (Springer Verlag, Berlin, 1992).
[9] H. Vrielinck, K. Sabbe, F. Callens, and P. Matthys, Phys. Chem. Chem. Phys. **3**, 1709 (2001).
[10] J. Owen and J. H. M. Thornley, Rep. Prog. Phys. **XXIX**, 676 (1966).
[11] S. V. Nistor, T. Pawlik, and J. M. Spaeth, J. Phys.: Condens. Matter **7**, 2225 (1995).
[12] E. Clementi and C. Roetti, At. Data Nucl. Data Tables **14**, 177 (1974).
[13] T. P. P. Hall, W. Hayes, R. W. H. Stevenson, and J. Wilkens, J. Chem. Phys. **39**, 35 (1963).
[14] C. G. Windsor, J. H. M. Thornley, J. H. E. Griffiths, and J. Owen, Proc. Phys. Soc. London **80**, 803 (1962).
[15] M. Tinkham, Proc. R. Soc. London, Ser. A **236**, 535 (1956).
[16] J. Casas-Gonzales, H. W. den Hartog, and R. Alcala, Phys. Rev. B **21**, 3826 (1980).
[17] P. Studzinski, J. Casas-Gonzales, and J. M. Spaeth, J. Phys. C **17**, 5411 (1985).
[18] J. A. Aramburu, P. Garcia-Fernandez, M. T. Barriuso, and M. Moreno, Phys. Rev. B **67**, 020101(R) (2003).
[19] H. Bill, Phys. Lett. **44**, 101 (1973).
[20] M. Moreno, Ann. Phys. (N.Y.) **70**, 261 (1974).
[21] P. Garcia-Fernandez, J. A. Aramburu, M. T. Barriuso, and M. Moreno, Phys. Rev. B **69**, 174110 (2004).